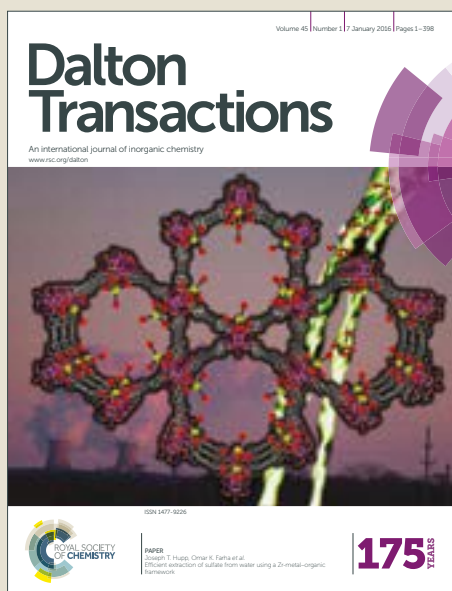


Dalton Transactions

Accepted Manuscript



This article can be cited before page numbers have been issued, to do this please use: Y. Zhang, S. zhang, Z. Tian, J. Li, Z. Xu, S. Li and Z. Liu, *Dalton Trans.*, 2018, DOI: 10.1039/C8DT03159B.



This is an Accepted Manuscript, which has been through the Royal Society of Chemistry peer review process and has been accepted for publication.

Accepted Manuscripts are published online shortly after acceptance, before technical editing, formatting and proof reading. Using this free service, authors can make their results available to the community, in citable form, before we publish the edited article. We will replace this Accepted Manuscript with the edited and formatted Advance Article as soon as it is available.

You can find more information about Accepted Manuscripts in the [author guidelines](#).

Please note that technical editing may introduce minor changes to the text and/or graphics, which may alter content. The journal's standard [Terms & Conditions](#) and the ethical guidelines, outlined in our [author and reviewer resource centre](#), still apply. In no event shall the Royal Society of Chemistry be held responsible for any errors or omissions in this Accepted Manuscript or any consequences arising from the use of any information it contains.



Journal Name

ARTICLE

Phenoxide Chelated Ir(III) N-Heterocyclic Carbene Complexes: Synthesis, Characterization, and Evaluation of the in Vitro Anticancer Activity

Received 00th January 20xx,
Accepted 00th January 20xx

DOI: 10.1039/x0xx00000x

www.rsc.org/

Yujiao Zhang, Shumiao Zhang*, Zhenzhen Tian, Juanjuan Li, Zhishan Xu, Shanshan Li, Zhe Liu*

Twelve novel half-sandwich Ir^{III}-NHC complexes [(η⁵-Cp^x)Ir(C[^]O)Cl] were synthesized and characterized. These complexes showed well cytotoxic activity toward A549 cells and HeLa cells than cisplatin. The more phenyl group contained, the better the anticancer activity appeared. The reaction of complexes with nucleobases 9-MeA, nucleobases 9-EtG, plasmid DNA and CT-DNA showed no significant effect. These complexes captured hydrogen from NADH and converted it to NAD⁺, which produced the ROS. ROS led to a decrease in mitochondrial membrane potential and lysosomal damage, and finally induced apoptosis.

Introduction

During the past several decades, it has been witnessed that transition metal complexes of N-heterocyclic carbenes (NHC) had developed a great deal,^{1,2} with high stability as one of their main characteristics.³ Besides wide use of the metal NHC complexes in catalysis,^{4,5} their application in medicinal and biological chemistry also plays an important role.⁶⁻⁹ As anticancer agents, platinum complexes such as cisplatin, carboplatin and oxaliplatin have achieved great success.¹⁰ Au and Ag complexes have illustrated considerable potential for development¹¹⁻¹³ and other transition metal compounds are also explored for their structure-activity relationships, such as ruthenium,¹⁴⁻²¹ palladium,²²⁻²⁴ osmium.^{25, 26} Recently, metal iridium complexes with the chelating ligand such as [N, N], [C, N], and [C, C] type showed better anticancer activity.²⁷⁻³⁵

In this paper, with the purpose of designing iridium NHC complexes as effective anticancer drugs, we tried to retain a carbene functionality, and added hard anionic building blocks because of its excellent stabilizing ability for Ir^{III}. The introduced anionic groups could reduce the dissociation of the ligand by enhancing the bond between the NHCs and the metal center.³⁶ Here we prepared twelve novel phenoxide chelated Ir^{III}-NHC complexes and studied these complexes for cell toxicity, hydrolysis chemistry, DNA binding, catalytic hydride transfer analysis, cell cycle, induction of apoptosis, reactive oxygen species induction, mitochondrial membrane assay and lysosomal damage. The results suggested that the twelve complexes had significant inhibitory effect on A549 cell proliferation than cisplatin and a preliminary understanding of their mechanisms of action. This work demonstrated that such class of

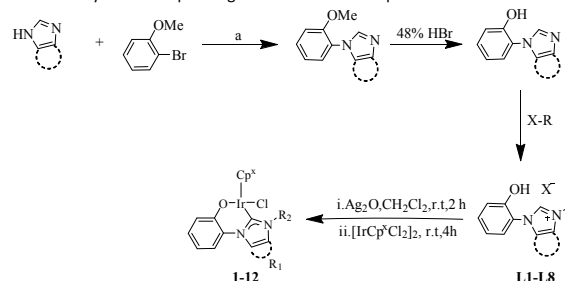
iridium complexes have potential to be new anticancer agents. To the best of our knowledge, this is the first report of this kind of half-sandwich Ir^{III} phenate chelated NHC complexes as anticancer drugs.

Results and discussion

Synthesis and Characterization

Ir^{III} complexes (**Chart 1**) of the type [(η⁵-Cp^x)Ir(C[^]O)Cl] were synthesized and characterized, where Cp^x includes Cp* and its biphenyl derivatives (Cp^x^{biph}), C[^]O-chelating ligands are NHC-phenoxide ligands. These complexes were obtained in a four step procedure (**Scheme 1**).^{37, 38} Initially the ligands were synthesized via copper catalyzed 1H-imidazole or 1H-benzimidazole with 2-bromoanisole in DMSO. Then the corresponding anisole derivative reacted with 48% HBr at reflux temperature for demethylation. Finally the desired salts were accomplished by reaction of 2-(1H-imidazol-1-yl) phenol or 2-(1H-benzimidazol-1-yl) phenol with a series of halogenated hydrocarbons at reflux temperature overnight. The target complexes were then obtained in a one-pot reaction by treating the respective ligand with Ag₂O followed by reaction with [IrCp^xCl₂]₂. These compounds were purified by filtration over celite and recrystallized. All complexes were characterized by ¹H NMR, ¹³C NMR, elemental analysis, and mass spectrometry.

Scheme 1. The Synthesis Steps of Ligands **L1 - L8** and Complexes **1 - 12**



a. 1H-imidazole and 2-bromoanisole reaction: K₂CO₃, CuO, DMSO, 150 °C, 10h; 1H-benzimidazole and 2-bromoanisole reaction: KOH, Cu₂O, DMSO, 150 °C, 24h.

Institute of Anticancer Agents Development and Theranostic Application, The Key Laboratory of Life-Organic Analysis and Key Laboratory of Pharmaceutical Intermediates and Analysis of Natural Medicine, Department of Chemistry and Chemical Engineering, Qufu Normal University, Qufu 273165, China.

*Corresponding author. Email: zkz_mao@163.com; liuzheqd@163.com

Electronic Supplementary Information (ESI) available.

See DOI: 10.1039/x0xx00000x

ARTICLE

Journal Name

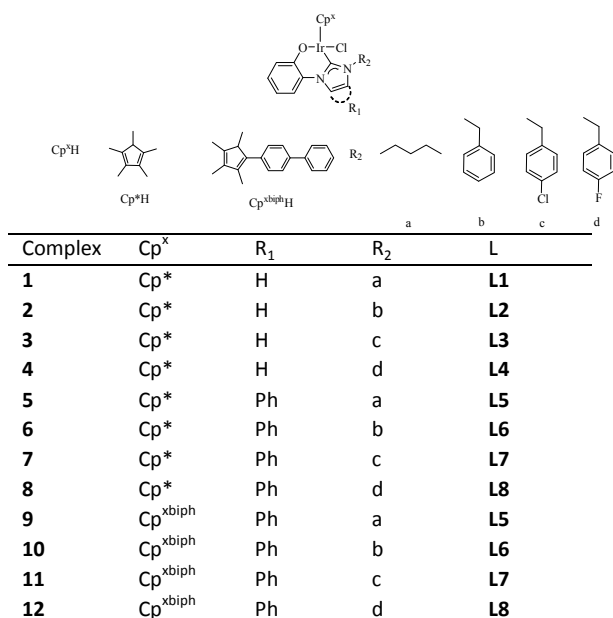
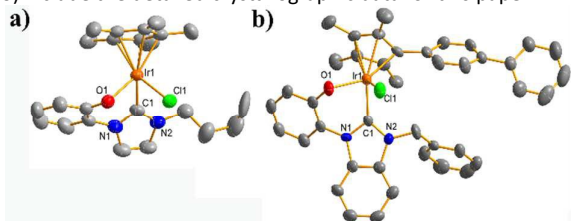


Chart 1. Iridium (III) complexes 1-12

X-ray crystal structures

Single crystals of complexes **1** and **10** (Fig. 1) were obtained by diffusion of n-hexane into CH₂Cl₂ solutions. Their structures were determined via the single-crystal X-ray diffraction analysis. The crystal data of complexes **1** and **10** were shown in Table 1 and Table 2. The crystal exhibited half-sandwich pseudo-octahedral, which proved the coordination of NHC and phenate groups with the iridium center. The observed Ir-C_{carbene} (2.019 Å and 2.002 Å, respectively) and Ir-O (2.096 Å and 2.104 Å, respectively) bond distance were in excellent agreement with those reported earlier for similar substances.³⁸ The distances from the iridium center to the η⁵-cyclopentadienyl centroid were respectively 1.7981 Å and 1.7994 Å for complexes **1** and **10**, both in the expected range.³⁹ And the Ir-Cl bond distances were respectively 2.4136 Å and 2.4079 Å in line with previous reports.³⁹ CCDC-1544033 (**1**) and CCDC-1852809 (**10**) include the detailed crystallographic data for this paper.

Fig. 1 X-ray crystal structure of complexes **1** (a) and **10** (b). Ellipsoids were 50% probability level and H atoms were omitted for clarity.Table 1. Crystal data and structure refinement for C₂₃H₃₀ClIrN₂O (**1**) and C₄₁H₃₆ClIrN₂O (**10**)

	Complex 1	Complex 10
formula	C ₂₃ H ₃₀ ClIrN ₂ O, CH ₂ Cl ₂	C ₄₁ H ₃₆ ClIrN ₂ O
MW	663.06	800.37
Temperature (K)	293(2) K	298(2) K
Crystal system	Triclinic	Monoclinic
space group	P-1	P2(1)/c
Crystal size	0.14×0.12×0.11 mm	0.30×0.18×0.14 mm
a (Å)	9.2934(19)	10.2202(9)
b (Å)	11.622(2)	15.4052(13)
c (Å)	13.674(3)	21.1662(18)

α (deg)	65.73(3)	90
β (deg)	80.57(3)	95.9780(10)
γ (deg)	74.82(3)	90
Volume (Å ³)	1296.8(6)	3314.37(49)
Z	2	4
density (Mg/m ³)	1.698	1.604
Absorption	5.475	4.145
coefficient (mm ⁻¹)		
reflns collected	9851	16304
indep reflns	6371	5827
	[R(int)=0.0354]	[R(int)=0.0796]
Final R indices	R1=0.0475,	R1=0.0446,
[>2σ(I)]	wR2 = 0.1177	wR2=0.1046

Table 2. Selected bond lengths [Å] and angles [deg] for C₂₃H₃₀ClIrN₂O (**1**) and C₄₁H₃₆ClIrN₂O (**10**)

	Complex 1	Complex 10
Ir1-C (cyclopentadienyl)	2.125(7)	2.132(7)
	2.133(7)	2.138(7)
	2.156(6)	2.163(7)
	2.220(6)	2.210(8)
	2.230(6)	2.220(7)
Ir1-C (centroid)	1.7981	2.002
Ir1-Cl1	2.019(6)	2.002(7)
Ir1-O1	2.096(5)	2.104(5)
Ir1-Cl1	2.4136(17)	2.4079(18)
C1-Ir1-O1	82.4(2)	83.5(2)
C1-Ir1-Cl1	89.3(2)	84.45(19)
O1-Ir1-Cl1	85.28(13)	83.34(14)

Cytotoxicity assay in vitro

The MTT assay is a widely used method of determining IC₅₀ (the half maximal inhibitory concentration) values for complexes of cancer cell lines. The A549 cell line and HeLa cell line have a degree of representativeness and stability, which provides accurate feedback on drug response. Complexes **1** - **12** had a significant inhibitory effect on A549 cells and HeLa cells proliferation than cisplatin. The IC₅₀ values of complexes **1-12** for A549 cells and HeLa cells ranged from 2.51-20.76 μM and 2.24-6.69 μM, respectively (Table 3), which were smaller than cisplatin (IC₅₀ = 21.30 μM, IC₅₀ = 7.50 μM). The IC₅₀ value of complex **6** were the smallest among the Cp* complexes, about 5 times and 2 times more potent than cisplatin for A549 cells and HeLa cells, respectively. The Cp^xbiph complexes showed higher antiproliferative activity than their Cp* analogs. We found that the activity of the complexes performed better as the number of phenyl groups in the complex increased. However, the anticancer activity did not seem to change a lot while halogens were added to the para-position on the benzyl group as compared to that of the benzyl group. Unfortunately, the IC₅₀ values of complexes **2** and **6** were small in the antiproliferative activity test of BEAS-2B human normal lung epithelial cells. This type of complexes did not show selectivity for cancer cells and normal cells.

Table 3. IC₅₀ values of complexes **1-12** and cisplatin towards A549 cells, HeLa cells and BEAS-2B

Complex	IC ₅₀ (μM) A549	IC ₅₀ (μM) HeLa	IC ₅₀ (μM) BEAS-2B
1	20.8±2.2	6.7±0.2	
2	16.7±2.2	5.6±0.2	2.5±0.2
3	16.5±0.8	5.9±0.1	
4	13.7±1.3	6.4±0.4	
5	8.5±0.9	4.0±0.7	
6	3.9±0.1	3.1±0.1	3.2±0.1
7	5.3±0.9	3.5±0.2	
8	5.4±0.4	3.6±0.4	
9	3.0±0.4	3.0±0.2	

10	2.5±0.6	2.6±0.2
11	2.6±0.1	2.4±0.1
12	3.3±0.5	2.2±0.5
Cisplatin	21.3±1.7	7.5±0.2

Hydrolysis studies

The hydrolysis ability was then studied, owing to the fact that the hydrolysis of M-Cl bonds to M-OH bonds indicated an activation step for transition metal anticancer complexes.³⁹ Complexes **2**, **4**, **5** and **6** were used as model. Hydrolysis of complex **4** was carried out at 310 K in 80% MeOD-d₄/20% D₂O (v/v) to monitor its changes by ¹H NMR (Fig. S2, ESI[†]). The methanol was used to dissolve the complex and ensure that the complex did not precipitate after the addition of water. The other complexes **2**, **5** and **6** were tested in the same way (Fig. S1, S3 and S4, ESI[†]). The change of the ¹H NMR spectroscopy was little compared 5 min with 24 h. In order to ensure that the complex did undergo a hydrolysis reaction, 16 mol equivalents NaCl were added to the solution after hydrolysis equilibrium. It was clear that the peak of the hydrated adducts disappears.

Hydrolysis kinetics of complexes **2**, **4**, **5** and **6** were studied by UV at 298 K in 20% MeOH/ 80% H₂O (v/v) (Fig. S5-S6, ESI[†]). Based on the formation of the hydrate adducts in accordance with the pseudo first order kinetics, we calculated the hydrolysis rate constant and half-lives (Table S1, ESI[†]). The results showed that the hydrolysis rates of complexes **2**, **4**, **5** and **6** were relatively rapid. These complexes rapidly underwent hydrolysis in water because of the replacement of the chloride ligand. According to what has been reported for similar Ir^{III} complexes containing Cl, in the case of hydrolysis, the other ligands are stable in addition to the substitution of Cl.⁴⁰ This indicates that the complexes have good stability in 80% MeOD-d₄/20% D₂O.

Solubility Experiment

The solubility of the complexes **2**, **4** and **6** were measured by the UV-spectroscopy.^{35, 41} The solution of complexes were prepared in DMSO with the concentration of 10 mM. The stock solutions were diluted in concentrations ranging from 5 × 10⁻⁶ to 5 × 10⁻⁴ mol/L in 80% HEPES (pH=7.2-7.4) and 20% acetonitrile. The acetonitrile acts as a cosolvent to prevent precipitation. The saturated solution of the complexes were monitored by the UV-spectroscopy. Complexes **2**, **4** and **6** had 301.68mg/L, 332.55 mg/L, and 48.79 mg/L, respectively (Fig. S7, ESI[†]). Complex **4** bearing F shows better solubility than complex **2**, while complex **2** has better solubility than complex **6** with more than one phenyl group.

Interaction with nucleobases

In the search for biomedical and anticancer drug mechanisms, DNA is regarded as a target for anticancer drugs.^{42, 43} In our study, the experiments of complexes **2**, **4**, **5** and **6** with 9-ethylguanine (9-EtG) and 9-methyladenine (9-MeA) were performed. Equilibrated solutions of complexes **2**, **4**, **5** and **6** (1.0 mM) in 80% MeOD-d₄ / 20% D₂O (v / v) were prepared at 310 K, to which then were added 1 mol equiv of 9-EtG or 9-MeA. From the Table S2, ESI[†], no formation of any nucleobase adducts were shown by ¹H NMR after 24 h.

Cleavage of plasmid DNA

We performed experiments on the ability of complexes to cleave DNA. Plasmid pBR322 DNA (10 μM) and various concentrations of **2**, **4**, **5** and **6** were incubated at 37 °C for 24 hours. The mixture was added to the sample tank of the prepared agarose gel using a micropipette. Then the contents were detected for 1 h by agarose Gel electrophoresis in TAE buffer (40 mM Tris-HCl/1 mM EDTA, pH=8.3). From Fig. S8, ESI[†], DNA cleavage with various concentrations of complexes **2**, **4**, **5** and **6** was not observed.

DNA binding

Then the complexes **2**, **4** and **6** with DNA binding were monitored by UV-Vis spectroscopy. Absorption titration experiments were performed by keeping a constant complex concentration (20 μM) and continuously adding CT-DNA concentration (0–108 μM) in the buffer. As seen from the Fig. S9, ESI[†], after adding to incremental amounts of CT-DNA, the absorption band of the three complexes showed hypochromism and a little bathochromism, displaying a little binding affinity to double stranded DNA. According to absorption spectral titration data, the binding constants *K_b* was calculated by the following equation.

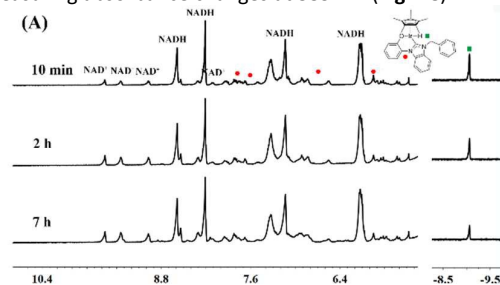
$$\frac{A_0}{A - A_0} = \frac{\epsilon_f}{(\epsilon_b - \epsilon_f)} + \frac{\epsilon_f}{K_b(\epsilon_b - \epsilon_f)[DNA]}$$

where *A*₀ and *A* respectively correspond to the initial absorbance of the free complex and absorbance of the complex in the presence of DNA, *ε_f* is the extinction coefficient of the free compound and *ε_b* is the extinction coefficient of the compound when fully bound to DNA. The curve of *A*₀/(*A* - *A*₀) versus 1/[DNA] gives the straight line and the *K_b* is calculated as the intercept / slope ratio (Table S3, ESI[†]). These spectral characteristics obviously suggest that these complexes interact with CT-DNA probably through a semi-intercalation or quasi-intercalation.

NADH catalytic reaction

The NAD⁺/NADH couple is an important redox couple in numerous biochemical reactions. Previously, Ir^{III} cyclopentadienyl complexes were reported that could interfere with NAD⁺/NADH hydrogen transfer reactions in cells and produce the ROS H₂O₂.^{44, 45} We did some related research of NAD⁺/NADH with complex **2**, **4**, **5** and **6** by NMR and UV-vis to investigate. The solution of complex **6** (1 mM) was prepared with 80% methanol and 20% water, then added NADH (3.5 mol equiv.). The change of NADH and complex **6** from 10 min to 7 h was monitored by NMR at 310 K. The ¹H NMR spectrum showed a new peak at 8.97, 9.35 and 9.56 ppm corresponding to the positions of the C4, C6 and C2 hydrogen atoms of the NAD⁺ nicotinamide ring, which indicated the conversion of NADH to NAD⁺ (Fig. 2A). Especially, a sharp single peak was observed at -9.06 ppm, which was the Ir-H bond (Fig. 2A). In addition, the reactions of NADH with complex **2**, **4** and **5** also had new peaks in the low field and a sharp single peak in the negative field (Fig. S10-S12, ESI[†]).

The catalytic ability of NADH with these complexes was monitored via UV-vis within 8 h in 10% MeOH / 90% H₂O at room temperature. In the UV spectrum, NADH showed absorption at 339 nm, whereas NAD⁺ did not. In Fig. 2B and Fig. S13, ESI[†], the absorbance at 339 nm decreased significantly after NADH reacting with complex **2**, **4**, **5** and **6**, which showing NADH was converted to NAD⁺. It was simple that the turnover numbers (TON) of complexes **2** (16.3), **4** (7.9), **5** (14.2) and **6** (23.5) were calculated according to measuring absorbance changes at 339 nm (Fig. 2C).



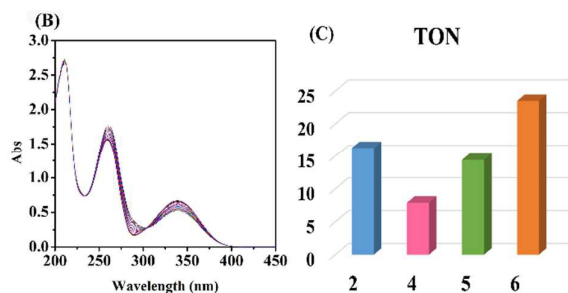


Fig. 2 (A) The reaction of complex **6** (1 mM) and NADH (3.5 mM) was monitored by ^1H NMR in 80%MeOD- d_4 /20% D_2O (v/v) at 310 K after 10 min, 2 h and 7 h. The peaks marked with \bullet represent the resulting formation of Ir-H complexes and \blacksquare correspond to the Ir-H hydrogen peak at -9.06 ppm (B) The reaction of complex **6** (1 μM) and NADH (100 μM) was monitored by UV-Vis spectrum in 10% MeOH/90% H_2O (v/v) at 298 K over 8 h. (C) the TONs of complexes **2**, **4**, **5** and **6**.

Cell cycle assay

Then the cell cycle progression was analyzed for complexes **2**, **4**, **6** and **12** treated A549 cells by flow cytometry. As shown in **Fig. S14-S15** and **Table S4-S7**, ESI^+ complex **2** and **12** resulted in increasing G_1 phase values. The values of G_1 phase of complex **2** treatment group varied from 57.81% to 69.67% with increasing treated concentration, the percentage of G_1 phase of complex **12** treatment group increased from 56.71% to 66.40%. For complex **4** and **6**, the percentage of the cell cycle did not significantly change as the concentration increasing.

Apoptosis assay

We further investigated apoptosis by flow cytometry and determined the percentages of apoptosis. A549 cells were treated with complexes **2**, **4**, **6** and **12** for 24 h, stained with the solution of annexin V/ propidium iodide (PI), followed by cell apoptosis analysis via flow cytometry. When A549 cells incubated with complex **2** at different concentrations, the percentage increased from 0.68% to 2.89% in early apoptotic cells and 6.71% to 51.11% in late apoptotic cells (**Fig. S16** and **Table S8**, ESI^+). For complex **4** at concentration of $3 \times \text{IC}_{50}$, cells were 7.17% in the early apoptotic phase and 44.49% in the late apoptotic phase (**Fig. S17** and **Table S9**, ESI^+). A549 cells treated with complex **6** showed no obvious changes in early apoptosis. At a concentration of $3 \times \text{IC}_{50}$, late apoptotic cells were 27.31%, and non-viable cells were 10.92% (**Fig. 3**, and **Fig. S18**, **Table S10**, ESI^+). When A549 cells treated with complex **12** at $3 \times \text{IC}_{50}$ after 24 h, the early apoptotic phase cells were 2.27% and the late apoptotic phase cells were 26.13% (**Fig. S20**, ESI^+ and **Table S12**, ESI^+). As shown in these figures and tables, more apoptotic cells were observed because of the increasing concentration of the complexes. Furthermore, A549 cells were treated with complex **6** for 12 hours, and the results are shown in the **Fig. S19** and **Table S11**, ESI^+ . Compared with 24 hours, the cells increased in early apoptosis after treatment with complex **6** for 12 hours. And the late apoptosis gradually increased as the concentration of the compound increased.

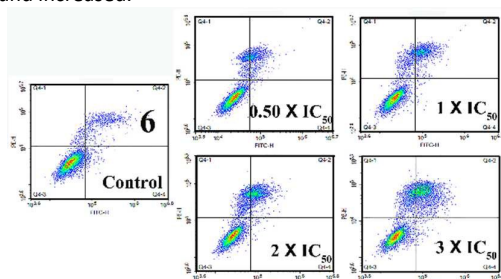


Fig. 3 Apoptosis of A549 cancer cells of exposure to complex **6** was detected by flow cytometry after 24 h at 310 K.

Reactive oxygen species

Reactive oxygen species (ROS) are mainly produced in mitochondria as products of cellular metabolism and closely related to apoptosis. ROS are typically generated by a redox cycle via electron transfer groups such as metal complexes.^{46, 47} Therefore, we performed ROS experiment and observed ROS levels in A549 cells treated with complexes **6** and **12** for 24 h. From **Fig. 4**, and **Fig. S21**, **Table S13**, ESI^+ , the ROS levels were significantly increased in the A549 cells after treatment with complexes **6** and **12**, and twice higher than in the negative controls.

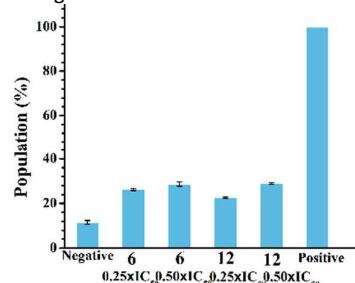


Fig. 4 ROS levels for A549 cells treated with complex **6** and **12** at $0.25 \times \text{IC}_{50}$ and $0.5 \times \text{IC}_{50}$ were analyzed by flow cytometry.

Induction of Mitochondrial Dysfunction

We previously reported experimental evidence that ruthenium complex affected the alteration of the mitochondrial membrane potential and might be related to anticancer activity.¹⁵ The mitochondrial membrane potential (MMP, $\Delta\Psi\text{m}$) implicated mitochondrial dysfunction and participated in induction apoptosis. We investigated the effects of complexes **2**, **4**, **6** and **12** (at concentrations of 0.25, 0.5, 1 and $2 \times \text{IC}_{50}$) on MMP in A549 cancer cells via JC-1 (a fluorescent probe). In the negative control, JC-1 emits red fluorescence, which corresponds to high MMP. In the positive control, A549 cells were with low MMP showing green fluorescence. From **Fig. 5**, and **Fig. S22-S25**, **Table S14-S17**, ESI^+ , the low MMP increased with the concentration increasing. Complexes **2**, **4**, **6** and **12** can induce a decrease in the MMP and appear a concentration-dependent manner.

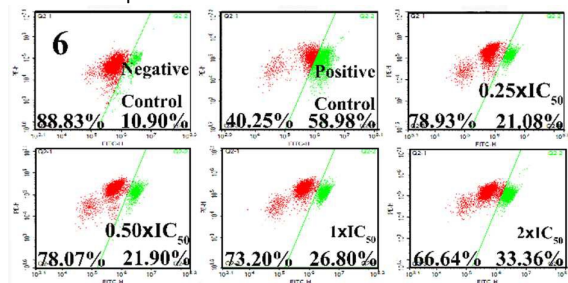


Fig. 5 Mitochondrial membrane potential of A549 cancer cells treatment with complex **6** at concentrations of 0.25, 0.5, 1 and $2 \times \text{IC}_{50}$ were determined by JC-1.

Lysosomal damage

Acridine orange (AO) is a fluorochrome which can effectively reflect the functional status of lysosomes. When AO enters cells and accumulates in lysosomes, the fluorescence emission is changed from cytosolic green to lysosomal red.⁴⁸ From the **Fig. S26**, ESI^+ , the green fluorescence of A549 cytoplasm increased and the red fluorescence decreased as increasing concentration of the complex **6**. The result indicated lysosomal membrane permeability was increased and lysosomes was damaged. In addition to causing increased mitochondrial membrane permeability and involvement in apoptosis, intracellular ROS could directly damage lysosomal membranes.⁴⁹

Conclusions

The development of metal-NHCs in medicinal and biological chemistry is very rapid. In this paper, we designed twelve phenoxide chelated Ir^{III}-NHC complexes and studied their anticancer activity.

Complexes **1-12** showed activity towards A549 cells and HeLa cells, especially these complexes had even higher inhibitory effect than cisplatin. Altering the complexes' structure may influence their anticancer activity. The tested complexes hydrolyzed in aqueous solution. However, these complexes displayed no binding to 9-MeA and 9-EtG and no cleavage to pBR322 DNA. They showed a little binding affinity to CT-DNA, probably through non-covalent binding modes. Thus, DNA may not be the primary target of these complexes. Complexes interfere with NADH/NAD⁺ hydrogen transfer, which produce the ROS. ROS level detection increased in the cells after addition complexes **6** and **12**. Complex **2** and **12** influenced the cell cycle at the G₀/G₁ phase. Apoptotic cells and mitochondrial dysfunction were observed, which may be contributed to anticancer activity. Complex **6** cause lysosomal damage through confocal microscopy observation. The findings demonstrated that half-sandwich Ir^{III}-NHC complexes converted NADH to NAD⁺, which produced the ROS. ROS level detection confirmed that ROS levels did increase. The production of ROS led to a decrease in mitochondrial membrane potential and lysosomal damage, and finally induced apoptosis.

All the results appear that phenoxide chelated Ir^{III}-NHC complexes [(η⁵-Cp*)Ir(C[^]O)Cl] have well anti-cancer effects. It is hoped that these type complexes will continue to be studied and become effective human anti-cancer drugs.

Conflicts of interest

There are no conflicts to declare.

Acknowledgements

We thank the National Natural Science Foundation of China (21671118), the Taishan Scholars Program and Shandong Provincial Natural Science Foundation (ZR2018LB007) for support.

Notes and references

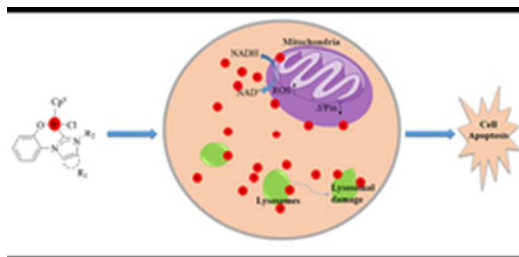
1. A. J. Arduengo and R. Kraczyk, *Chem. unserer Zeit*, 1998, **32**, 6-14.
2. M. N. Hopkinson, C. Richter, M. Schedler and F. Glorius, *Nature*, 2014, **510**, 485-496.
3. D. Bourissou, O. Guerret, F. P. Gabbaï and G. Bertrand, *Chem. Rev.*, 2000, **100**, 39-92.
4. W. A. Herrmann, *Angew. Chem. Int. Ed.*, 2002, **41**, 1290-1309.
5. J. A. Mata, F. E. Hahn and E. Peris, *Chem. Sci.*, 2014, **5**, 1723-1732.
6. K. M. Hindi, M. J. Panzner, C. A. Tessier, C. L. Cannon and W. J. Youngs, *Chem. Rev.*, 2009, **109**, 3859-3884.
7. L. Mercs and M. Albrecht, *Chem. Soc. Rev.*, 2010, **39**, 1903-1912.
8. A. Gautier and F. Cisnetti, *Metallomics*, 2012, **4**, 23-32.
9. L. Oehninger, R. Rubbiani and I. Ott, *Dalton Trans.*, 2013, **42**, 3269-3284.

10. T. C. Johnstone, K. Suntharalingam and S. J. Lippard, *Chem. Rev.*, 2016, **116**, 3436-3486.
11. S. K. Fung, T. Zou, B. Cao, P.-Y. Lee, Y. M. E. Fung, D. Hu, C.-N. Lok and C.-M. Che, *Angew. Chem.*, 2017, **129**, 3950-3954.
12. T. Zou, C. T. Lum, S. S.-Y. Chui and C.-M. Che, *Angew. Chem. Int. Ed.*, 2013, **52**, 2930-2933.
13. S. J. Allison, M. Sadiq, E. Baronou, P. A. Cooper, C. Dunnill, N. T. Georgopoulos, A. Latif, S. Shepherd, S. D. Shnyder, I. J. Stratford, R. T. Wheelhouse, C. E. Willans and R. M. Phillips, *Cancer Lett.*, 2017, **403**, 98-107.
14. H. Huang, P. Zhang, Y. Chen, K. Qiu, C. Jin, L. Ji and H. Chao, *Dalton Trans.*, 2016, **45**, 13135-13145.
15. M. Tian, J. Li, S. Zhang, L. Guo, X. He, D. Kong, H. Zhang and Z. Liu, *Chem. Commun.*, 2017, **53**, 12810-12813.
16. S. Thota, D. A. Rodrigues, D. C. Crans and E. J. Barreiro, *J. Med. Chem.*, 2018, **61**, 5805-5821.
17. S. Thota and D. Crans, *Introduction: Synthesis and Applications in Pharmaceutical Sciences*, 2017.
18. Y. Yang, G. Lihua, Z. Tian, X. Liu, Y. Gong, H. Zheng, X. Ge and Z. Liu, *Chem. Asian J.*, 2018, DOI: 10.1002/asia.201801058.
19. Q. Du, L. Guo, M. Tian, X. Ge, Y. Yang, X. Jian, Z. Xu, Z. Tian and Z. Liu, *Organometallics*, 2018, DOI: 10.1021/acs.organomet.8b00402.
20. Z. Xu, D. Kong, X. He, L. Guo, X. Ge, X. Liu, H. Zhang, J. Li, Y. Yang and Z. Liu, *Inorg. Chem. Front.*, 2018, DOI: 10.1039/C8QI00476E.
21. Z. Tian, J. Li, S. Zhang, Z. Xu, Y. Yang, D. Kong, H. Zhang, X. Ge, J. Zhang and Z. Liu, *Inorg. Chem.*, 2018, DOI: 10.1021/acs.inorgchem.8b01944.
22. E. Z. Jahromi, A. Divsalar, A. A. Saboury, S. Khaleghizadeh, H. Mansouri-Torshizi and I. Kostova, *J. Iran. Chem. Soc.*, 2016, **13**, 967-989.
23. T. Zou, C.-N. Lok, P.-K. Wan, Z.-F. Zhang, S.-K. Fung and C.-M. Che, *Curr. Opin. Chem. Biol.*, 2018, **43**, 30-36.
24. M. Z. Ghahayeb, R. A. Haque, S. Budagumpi, M. B. Khadeer Ahamed and A. M. S. A. Majid, *Inorg. Chem. Commun.*, 2017, **75**, 41-45.
25. R. J. Needham, C. Sanchez-Cano, X. Zhang, I. Romero-Canelón, A. Habtemariam, M. S. Cooper, L. Meszaros, G. J. Clarkson, P. J. Blower and P. J. Sadler, *Angew. Chem. Int. Ed.*, 2017, **56**, 1017-1020.
26. C. Sanchez-Cano, I. Romero-Canelón, Y. Yang, I. J. Hands-Portman, S. Bohic, P. Cloetens and P. J. Sadler, *Chem. Eur. J.*, 2017, **23**, 2512-2516.
27. J. M. Hearn, I. Romero-Canelón, B. Qamar, Z. Liu, I. Hands-Portman and P. J. Sadler, *ACS Chem. Biol.*, 2013, **8**, 1335-1343.
28. D.-L. Ma, S. Lin, W. Wang, C. Yang and C.-H. Leung, *Chem. Sci.*, 2017, **8**, 878-889.
29. D.-L. Ma, C. Wu, W. Tang, A.-R. Gupta, F.-W. Lee, G. Li and C.-H. Leung, *J. Mater. Chem. B*, 2018, **6**, 537-544.
30. H. Zhang, L. Guo, Z. Tian, M. Tian, S. Zhang, Z. Xu, P. Gong, X. Zheng, J. Zhao and Z. Liu, *Chem. Commun.*, 2018, **54**, 4421-4424.
31. Z. Liu, I. Romero-Canelón, A. Habtemariam, G. J. Clarkson and P. J. Sadler, *Organometallics*, 2014, **33**, 5324-5333.
32. C. Wang, J. Liu, Z. Tian, M. Tian, L. Tian, W. Zhao and Z. Liu, *Dalton Trans.*, 2017, **46**, 6870-6883.
33. J. Li, M. Tian, Z. Tian, S. Zhang, C. Yan, C. Shao and Z. Liu, *Inorg. Chem.*, 2018, **57**, 1705-1716.

ARTICLE

Journal Name

34. W. Ma, Z. Tian, S. Zhang, X. He, J. Li, X. Xia, X. Chen and Z. Liu, *Inorg. Chem. Front.*, 2018, DOI: 10.1039/C8QI00620B.
35. T.-S. Kang, W. Wang, H.-J. Zhong, Z.-Z. Dong, Q. Huang, S. W. F. Mok, C.-H. Leung, V. K. W. Wong and D.-L. Ma, *Cancer Lett.*, 2017, **396**, 76-84.
36. Y. Kong, S. Xu, H. Song and B. Wang, *Organometallics*, 2012, **31**, 5527-5532.
37. S. Zhang, X. Li, H. Sun, O. Fuhr and D. Fenske, *J. Organomet. Chem.*, 2016, **820**, 41-45.
38. D. Gülcemal, S. Gülcemal, C. M. Robertson and J. Xiao, *Organometallics*, 2015, **34**, 4394-4400.
39. Z. Liu, A. Habtemariam, A. M. Pizarro, S. A. Fletcher, A. Kisova, O. Vrana, L. Salassa, P. C. A. Bruijninx, G. J. Clarkson, V. Brabec and P. J. Sadler, *J. Med. Chem.*, 2011, **54**, 3011-3026.
40. C. Mari, H. Huang, R. Rubbiani, M. Schulze, F. Würthner, H. Chao and G. Gasser, *Eur. J. Inorg. Chem.*, 2017, **2017**, 1745-1752.
41. B. Hoelke, S. Gieringer, M. Arlt and C. Saal, *Anal. Chem.*, 2009, **81**, 3165-3172.
42. N. Deepika, C. S. Devi, Y. P. Kumar, K. L. Reddy, P. V. Reddy, D. A. Kumar, S. S. Surya and S. Satyanarayana, *J. Photochem. Photobiol., B*, 2016, **160**, 142-153.
43. A. Kosiha, C. Parthiban and K. P. Elango, *J. Photochem. Photobiol., B*, 2017, **168**, 165-174.
44. Z. Liu, R. J. Deeth, J. S. Butler, A. Habtemariam, M. E. Newton and P. J. Sadler, *Angew. Chem. Int. Ed.*, 2013, **52**, 4194-4197.
45. S. Betanzos-Lara, Z. Liu, A. Habtemariam, A. M. Pizarro, B. Qamar and P. J. Sadler, *Angew. Chem. Int. Ed.*, 2012, **51**, 3897-3900.
46. S. Prasad, S. C. Gupta and A. K. Tyagi, *Cancer Lett.*, 2017, **387**, 95-105.
47. Paul T. Schumacker, *Cancer Cell*, 2015, **27**, 156-157.
48. J. Wang, Y. Yu, K. Lu, M. Yang, Y. Li, X. Zhou and Z. Sun, *Int. J. Nanomedicine.*, 2017, **12**, 809-825.
49. M. B. Azad, Y. Chen and S. B. Gibson, *Antioxid. Redox Sign.*, 2008, **11**, 777-790.



10x5mm (600 x 600 DPI)